

The 21-cm Signature of the First Stars

Xuelei Chen

National Astronomical Observatories, Chinese Academy of Sciences, Beijing 100012, China
xuelelei@bao.ac.cn

Jordi Miralda-Escudé

Institut de Ciències de l'Espai (CSIC-IEEC)/ICREA, 08193-Bellaterra, Spain
and
Department of Astronomy, The Ohio State University, Columbus OH 43210, USA
miralda@ieec.uab.es

ABSTRACT

We predict the 21-cm signature of the first metal-free stars. The soft X-rays emitted by these stars penetrate the atomic medium around their host halos, generating Ly α photons that couple the spin and kinetic temperatures. These creates a region we call the *Ly α sphere*, visible in 21-cm against the CMB, which is much larger than the HII region produced by the same star. The spin and kinetic temperatures are strongly coupled before the X-rays can substantially heat the medium, implying that a 21-cm absorption signal from the adiabatically cooled gas in Hubble expansion around the star is expected when the medium has not been heated previously. A central region of emission from the gas heated by the soft X-rays is also present although with a weaker signal than the absorption. The Ly α sphere is a universal signature that should be observed around any first star illuminating its vicinity for the first time. The 21-cm radial profile of the Ly α sphere can be calculated as a function of the luminosity, spectrum and age of the star. For a star of a few hundred M_{\odot} and zero metallicity (as expected for the first stars), the physical radius of the Ly α sphere can reach tens of kiloparsecs. The first metal-free stars should be strongly clustered because of high cosmic biasing; this implies that the regions producing a 21-cm absorption signal may contain more than one star and will generally be irregular and not spherical, because of the complex distribution of the gas. We discuss the feasibility of detecting these Ly α spheres, which would be present at redshifts $z \sim 30$ in the cold dark matter model. Their observation would represent a direct proof of the detection of a first star.

Subject headings: cosmology:theory — galaxies:formation — radiation mechanism:general — radio lines:general

1. Introduction

The formation of the first stars marks the end of the cosmic dark age and the beginning of the reionization era. The cold dark matter model with a cosmological constant (Λ CDM) of structure formation predicts that the first stars were formed in dark matter halos of $\sim 10^6 M_{\odot}$, which were sufficiently massive to allow the halo gas to collapse and cool through emission in molecular

hydrogen roto-vibrational lines (for reviews see, e.g., Barkana & Loeb 2001; Miralda-Escudé 2003; Ciardi & Ferrara 2005). Numerical simulations and analytic arguments suggest that in the absence of heavy elements, the gas in the halo center will cool hydrostatically and collapse into a central object when the Jeans mass is $\sim 10^3 M_{\odot}$, probably resulting in the formation of one or a few stars with $\sim 100 M_{\odot}$ (Bromm, Coppi, & Larson 1999; Abel, Bryan, Norman 2000; Omukai & Palla 2003).

Stars of this mass live for only 3×10^6 yr (Bromm, Kudritzki & Loeb 2006; Pritchard & Furlanetto 2006). At the end of their lives the supernova explosions enrich the intergalactic medium with heavy elements, which accelerate the cooling process and allow less massive stars to form. The reionization of the medium advances as more sources of ionizing radiation (stars or black holes emitting light as quasars) are formed in increasingly massive halos.

A very powerful observational probe of the end of the dark age is 21-cm tomography, which provides information on the state of the atomic intergalactic medium (IGM) (Madau, Meiksin, & Rees 1997; Tozzi et al. 2000, for a recent review see e.g. Furlanetto, Oh & Briggs 2006). Hydrogen atoms interact with 21-cm photons by radiative transitions between the hyperfine split ground state. The hydrogen may be seen in emission or absorption against the Cosmic Microwave Background (CMB) depending on whether its spin temperature is above or below the CMB temperature. The spin temperature is a weighted average of the gas kinetic temperature and the CMB temperature: it is driven toward the CMB temperature by the 21-cm transitions, and towards the kinetic temperature by atomic collisions and by resonant scattering of Ly α photons (Wouthuysen 1952; Field 1959). During the dark age (before the appearance of sources of light such as stars or accreting black holes), the kinetic temperature drops below the CMB temperature because of adiabatic cooling¹, and collisional coupling of the spin and kinetic temperatures can produce an absorption signal (Loeb & Zaldarriaga 2004; Barkana & Loeb 2005b; Naoz & Barkana 2005). Collisional coupling becomes ineffective below a redshift ~ 40 , except in high density regions such as collapsed minihalos (Iliev et al 2002; Kuhlen et al 2006). At lower redshift, the gas may again appear in absorption when illuminated with the Ly α photons from the first sources, which also couple the spin and kinetic temperatures through the Wouthuysen-Field mechanism (Chen & Miralda-Escudé 2004;

at the same time, the ionizing photons from the same first sources start heating the neutral medium, due mainly to soft X-rays which penetrate deeper into the atomic regions (Chen & Miralda-Escudé 2004; Sethi 2005). The 21-cm fluctuations are then due to variations of neutral density, Ly α flux and spin temperature (Barkana & Loeb 2005a). As reionization proceeds, X-rays heat the kinetic temperature to values much higher than the CMB temperature, and at the same time a Ly α photon background is produced which strongly couples the spin and kinetic temperatures. The 21-cm fluctuations are then essentially proportional to the density of neutral hydrogen, dependent on the IGM density and the ionization state (Madau, Meiksin, & Rees 1997; Ciardi & Madau 2003; Furlanetto, Sokasian, & Hernquist 2004; Kohler et al 2005).

In the present work, we study the 21-cm signature of the first stars, when the region around a star is illuminated by Ly α photons for the first time after the recombination epoch. Before a Ly α photon background is created, the spin temperature is close to that of the CMB temperature at most spatial locations. However, near a first star, the Ly α photon flux is strong enough to change the spin temperature, rendering the medium observable with 21-cm tomography. This region is substantially greater than the HII region generated by the star and the virial radius of the star-forming halo, as we shall see below. We shall refer to such a region as a *Ly α sphere*. The gas in the inner part of a Ly α sphere is heated up quickly by the radiation of the star (which, owing to the surface temperature $T_{eff} \simeq 10^5$ K of massive, metal-free stars, emits substantial soft X-rays during the main-sequence lifetime) to a temperature above T_{CMB} . Therefore, this inner region produces instead a core of 21-cm emission. The heating rate is much lower at the outer part of the Ly α sphere. Depending on the spectrum and the age of the star, the gas in the outer part of the Ly α sphere should appear as a halo of 21-cm absorption. This outer halo of absorption is not present if the region has been illuminated before by a sufficiently strong background of soft X-rays, and therefore heated by other more distant sources prior to the appearance of the star. Therefore, the detection of the absorption halo provides a unique signature

¹This picture of dark age would be drastically changed if non-conventional source of light, e.g. decaying dark matter, were present. For discussions on the state of IGM and 21cm signal in such cases, see, e.g., Chen & Kamionkowski (2004); Furlanetto, Oh & Pierapoli (2006); Ripamonti, Mapelli, Ferrara (2007); Valdes et al. (2007).

of a first star.

As this work was being completed, we became aware of the work by Cen (2006) along similar lines. Our conclusions differ from those of Cen in two respects: first, we find that Ly α spheres of absorption would be produced only around the very first sources of light in the universe, which should be metal-free stars (see, e.g. Abel, Bryan, & Norman 2002, Bromm & Larson 2004). At later times, the medium should be rapidly heated by X-rays and a global Ly α background should be produced, eliminating the Ly α spheres. Second, the most important source of Ly α photons that couple the spin and kinetic temperatures around a first star are not the continuum photons from the stellar photosphere, but the secondary Ly α photons due to impact excitations by electrons produced by the X-rays themselves. As we shall see in this paper, this fact is essential for improving the observability of these Ly α spheres in 21-cm absorption, by increasing their contrast relative to the background.

In §2, we derive the properties of an individual Ly α sphere. In §3 we investigate the formation history of the first stars. The growth of the Ly α and soft X-ray backgrounds, which affect the global evolution of the kinetic and spin temperature of the IGM, is considered in §4. In §5, we consider the observability of these Ly α spheres. We summarize our results in §6. In the following, we have adopted the WMAP three year Λ CDM model, with $h = 0.73$, $\Omega_m = 0.23$, $\Omega_b = 0.047$, $n_s = 0.99$, $\sigma_8 = 0.77$.

2. Properties of Ly α spheres

2.1. Basic concepts and notation

The form of the Ly α sphere produced around a first star, detectable by means of the 21-cm emission and absorption, is determined by the intensity of Ly α photons and soft X-rays produced over the history of the stellar lifetime. As a result of the irradiation of the neutral medium by stellar ultraviolet light, Ly α photons are produced by two mechanisms: they may have been emitted directly from the stellar photosphere at a frequency in the range between Ly α and Ly β and then redshifted to Ly α , or they may result from ionizing photons which can ionize hydrogen atoms that subsequently recombine and also excite other hydrogen atoms

with the energetic electrons created in the ionizations. Following Chen & Miralda-Escudé (2004), we designate the first type *continuum* photons, since they enter the Ly α line from the continuum spectrum on the blue wing of the line, and the second type *injected* photons, since they are injected close to the line center by an atom that has recombined or has been excited by a secondary electron, and has then reached the 2p state. We note that injected photons may also originate from photons emitted between the Ly γ line and the Lyman limit by the star, which will be absorbed by a hydrogen as they reach a Lyman resonant line, and may then produce a Ly α photon if the hydrogen atom cascades down to 2p. However, the majority of these photons result in a cascade that ends in the 2s state instead, so these typically make a small contribution to the creation of injected Ly α photons compared to the ionizing photons (see Hirata 2006; Pritchard & Furlanetto 2006).

A fixed point in the intergalactic medium can be reached by continuum photons from stars out to a maximum redshift of $z_{c,max} = (8/9)/(3/4) - 1 = 5/27$. Injected photons from ionization may come from a higher redshift, but they need to arise from X-rays which can penetrate over a large distance in the atomic medium. Every X-ray can produce several secondary ionizations and collisional excitations by the electrons that are produced, and these will result in the production of a Ly α photon when the hydrogen atom reaches the 2p (rather than the 2s) state. These Ly α photons start scattering after they are produced, and they are confined to a very small region of the universe owing to the large cross section for Ly α scattering in the neutral medium. The flux of Ly α photons at any point in the atomic intergalactic medium is therefore related to the local flux of X-rays and continuum photons between the Lyman series lines coming from distant stars, although some spatial diffusion of the Ly α photons may take place in the last few scatterings, when the photon exits the Ly α line (Loeb & Rybicki 1999).

The brightness temperature of 21-cm photons is given by

$$\delta T_b = 40\text{mK} \left(\frac{\Omega_b h_0}{0.03} \right) \left(\frac{0.3}{\Omega_{m0}} \right)^{1/2} \left(\frac{1+z}{25} \right)^{1/2} \times \frac{\rho_{HI}}{\bar{\rho}_H} \frac{T_s - T_{CMB}}{T_s}. \quad (1)$$

The spin temperature T_s is a weighted average of the CMB temperature and the gas kinetic temperature, and can be approximately calculated as (see Hirata 2006 for a more exact treatment)

$$T_S = \frac{T_{CMB} + (y_\alpha + y_c)T_k}{1 + y_\alpha + y_c} \quad (2)$$

where the coupling coefficients y_α and y_c are proportional to the Ly α scattering rate (Wouthuysen 1952; Field 1959) and spin-changing collision rate, respectively:

$$y_\alpha = \frac{P_{10}T_*}{A_{10}T_k}, \quad y_c = \frac{C_{10}T_*}{A_{10}T_k}. \quad (3)$$

Here, $T_* = 0.068\text{K}$ is the temperature corresponding to the energy of the hyperfine structure of hydrogen, $A_{10} = 2.87 \times 10^{-15} \text{ s}^{-1}$ is the Einstein coefficient of the hyperfine structure levels, and C_{10} is the collisional de-excitation rate (tabulated first by Allison & Dalgarno (1969), and more recently by Zygelman (2005); Furlanetto & Furlanetto (2007a,b); in this paper we use the tabulated values given by Furlanetto, Oh & Briggs (2006)). The spin-flip transition rate P_{10} is given by

$$P_{10} = \frac{4}{27} H \tau_{GP} \frac{S_c J_c + S_i J_i}{\tilde{J}_0}, \quad (4)$$

where H is the Hubble rate at that redshift, τ_{GP} is the Gunn-Peterson optical depth, J_c and J_i are the intensities of continuum and injected Ly α photons, and S_c and S_i are numerical factors of order unity that depend on the gas temperature and on τ_{GP} (see Chen & Miralda-Escudé (2004); Hirata (2006)²). In the high temperature limit, $S_{c,i} \rightarrow 1$. For simplicity, in the present paper we shall assume $S_c = S_i$, and use the value as given by the fitting formula of Furlanetto & Pritchard (2006). The fiducial intensity \tilde{J}_0 corresponds to a photon density of one photon per hydrogen atom per log frequency,

$$\tilde{J}_0 = \frac{cn_H}{4\pi\nu_\alpha}, \quad (5)$$

²The numerical values of the heating and collisional rate coefficients I_i , I_c , S_i, S_c given in Chen & Miralda-Escudé (2004) are all too large by a factor of $\sqrt{\pi}$, because of an incorrect normalization used in the original code (this does not affect the basic conclusions reached in Chen & Miralda-Escudé (2004)). We thank Chris Hirata for pointing out this error to us. Also, loss of Ly α photons by the two photon decay process could further reduce the effective collision rate slightly, see Hirata (2006) for further information.

where n_H is the number density of hydrogen and ν_α is the frequency of Ly α . In ordinary units, $\tilde{J}_0 h\nu_\alpha = 2.69 \times 10^{-24} \times (1+z)^3 (\Omega_b h_0^2 / 0.02) \text{ erg cm}^{-2} \text{ s}^{-1} \text{ sr}^{-1} \text{ Hz}^{-1}$. At $z \sim 20 - 30$, $y_\alpha \sim 1$ when $J/\tilde{J}_0 \sim 0.02$.

2.2. Ly α sphere model

The Ly α sphere of a first star is the region where the spin temperature is substantially modified by the Ly α photon flux arriving from the star, producing an observable signature in the 21-cm line. Stars that form later emit their ultraviolet light into a region that has already been previously illuminated by a background of light from more distant stars which formed earlier, and the contrast of the Ly α sphere from an individual star will of course rapidly diminish as the background intensity increases. In this paper, we designate as “first star” any star that emits the first light into the atomic medium that surrounds it. Many more metal-free stars form later from pristine material (i.e., not contaminated by any stellar ejecta), but which has been illuminated by stellar light; these stars create a Ly α sphere in the presence of a light background, with lower contrast. Note that the region around a star is also modified by an increased kinetic temperature due to ionization by soft X-rays.

In this paper we assume that all the first stars are massive (Bromm & Larson 2004), with masses ranging from $25 M_\odot$ to $800 M_\odot$. The main sequence lifetime of a massive, metal-free star is about three million years, and is generally much longer than the Kelvin-Helmholz time to reach the main-sequence. We treat the stars as static during their lifetime, with constant luminosity. As we shall see below, due to the r^{-2} decrease of the photon flux, the size of Ly α sphere is typically limited to a few tens of kpc, so the corresponding light propagation time is also negligible compared with the stellar lifetime. The scale of this Ly α sphere is much greater than the halo harboring the star, so we treat the density of the gas as uniform and equal to the cosmic mean (note that this may be inaccurate in many cases because of the highly biased large-scale distribution of the first stars). The flux of the stellar continuum per unit frequency is

$$J_c = \frac{L(\nu_\alpha)}{(4\pi)^2 r_p^2} \quad (6)$$

where r_p is the physical distance to the star, and $L(\nu)$ is the stellar luminosity per unit frequency. We model the stellar radiation as blackbody with surface temperature and total luminosity given by (Bromm, Kudritzki & Loeb 2001)

$$T = 1.1 \times 10^5 \left(\frac{M}{100M_\odot} \right)^{0.025} K \quad (7)$$

$$L_{total} = 10^{4.5} \frac{M}{M_\odot} L_\odot \quad (8)$$

2.3. Ionization and heating of the Ly α sphere

We now proceed to solve for the ionization fraction, kinetic temperature, spin temperature, and the 21-cm emission temperature around the star. We include recombinations in our calculation, but as the recombination time at the average density of the universe is a few times longer than the lifetime of the star and its associated Ly α sphere, it does not have a big impact on our result. Note that we are also assuming that the high-density halo gas around the star (which does not have time to be ejected from the halo during the stellar lifetime after it is ionized and heated) does not absorb a large fraction of the stellar ionizing photons emitted by the central star (Whalen, Abel, & Norman 2004). We also do not consider ionization and heating by any X-ray background that may have been produced by sources other than the star. The neutral fraction is determined by

$$\frac{dx_{\text{HI}}}{dt} = -x_{\text{HI}} \int_{\nu_{\text{H}}}^{\infty} d\nu F(\nu) \sigma_{\text{HI}}(\nu) + \alpha_B^{\text{H}} x_{\text{HI}} x_e n_{\text{H}} \quad (9)$$

$$\frac{dx_{\text{HeI}}}{dt} = -x_{\text{HeI}} \int_{\nu_{\text{HeI}}}^{\infty} d\nu F(\nu) \sigma_{\text{HeI}}(\nu) + \alpha_B^{\text{HeI}} x_{\text{HeI}} x_e n_{\text{He}} \quad (10)$$

$$\frac{dx_{\text{HeII}}}{dt} = -\frac{dx_{\text{HeI}}}{dt} - x_{\text{HeII}} \int_{\nu_{\text{HeII}}}^{\infty} d\nu F(\nu) \sigma_{\text{HeII}}(\nu) + \alpha_B^{\text{HeII}} x_e (1 - x_{\text{HeI}} - x_{\text{HeII}}) n_{\text{He}} \quad (11)$$

Here, $F(\nu)$ is the flux of ionizing photons per unit frequency, n_{H} and n_{He} are the total number density of H and He atoms, and x_i , $\sigma_i(\nu)$, and ν_i are the fractional abundance, the cross section and the ionization threshold frequency of each atom or ion of type i , respectively. The case B recombination rates for hydrogen α_B^{H} is calculated by using the fitting formula given in Hummer & Seaton

(1963), the α_B^{HeI} , α_B^{HeII} are calculated by interpolating/extrapolating the tabulated values given in Storey & Hummer (1995); Hummer & Storey (1998). In the helium ionization, we have neglected the contribution of direct double ionization, as this rate is small compared with ionization in two stages. We fit the cross sections using the functions given in Verner et al. (1996). The flux at physical distance r_p is given by

$$F(\nu) = \frac{L(\nu)}{4\pi r_p^2} e^{-\tau(\nu)} \quad (12)$$

where

$$\begin{aligned} \tau(\nu) = & n_{\text{H}} \sigma_{\text{HI}}(\nu) \int_0^r dr' x_{\text{HI}}(r') \\ & + n_{\text{He}} \sigma_{\text{HeI}}(\nu) \int_0^r dr' x_{\text{HeI}}(r') \\ & + n_{\text{He}} \sigma_{\text{HeII}}(\nu) \int_0^r dr' x_{\text{HeII}}(r') \end{aligned} \quad (13)$$

We assume $x_{\text{HI}} = x_{\text{HeI}} = 2 \times 10^{-4}$, $x_{\text{HeII}} = 0$ everywhere initially (to include the primordial ionization). We then evolve the ion fractions on a lattice of 200 points (logarithmically distributed from $r = 0.01\text{kpc}$ to $r = 100\text{kpc}$) with the above differential equations. The solution of the ordinary differential equation is obtained with a predictor-corrector scheme (Engeln-Mullges & Uhlig 1996).

The internal energy of the gas is given by

$$U = \frac{3}{2} [n_{\text{H}}(2 - x_{\text{HI}}) + n_{\text{He}}(3 - 2x_{\text{HeI}} - x_{\text{HeII}})] kT \quad (14)$$

The volume heating rate $\Gamma = \frac{dU}{dt}$ is given by

$$\Gamma = \sum_{i=\text{HI,HeI,HeII}} n_i \int_{\nu_i}^{\infty} d\nu h(\nu - \nu_i) \eta(x, \nu) F(\nu) \sigma_i(\nu), \quad (15)$$

where the fraction of photo-electron energy converted to heat $\eta(x, \nu)$ is a function of energy and free electron fraction. Shull & van Steenberg (1981) calculated this function using a Monte Carlo simulation, and found that it can be fitted as

$$\eta = 0.9971(1 - (1 - x^{0.2663})^{1.3163}). \quad (16)$$

Note that this fit breaks down at very low x , but it is a good approximation for $x \gtrsim 10^{-4}$. Also, this fitting function was obtained for non-primordial

helium abundance, so the real result may differ slightly.

At large r_p , where the ionized fraction in the Ly α sphere is low, cooling is negligible and we simply calculate the temperature using the above expressions for calculating the internal energy and the heating rate, assuming that there is no cooling. The effect of atomic cooling sets in rather abruptly once the temperature reaches $T \simeq 10^4$ K, and we assume that the temperature stays fixed at this value after it is reached. This does not affect our result on 21-cm because at these high temperatures the emission depends only on the hydrogen column density.

2.4. Secondary Ly α photons from ionization by X-rays

Owing to the high temperature of the metal-free stars, the soft X-rays from the stellar photosphere result in a substantial ionization and heating ahead of the thin shell where most of the ionization occurs. These high-energy electrons produced by the X-rays that penetrate into the mostly atomic zone also result in the emission of additional Ly α photons: in the limit of low fractional ionization and high photon energy, a fraction $\eta_\alpha \sim 40\%$ of the X-ray energy is converted to photons through excitation by the high-energy electrons. Here we assume all of these are in Ly α photons. In reality, the fraction may be slightly smaller. The intensity of these Ly α photons is added to those coming from the stellar photosphere and can contribute to the coupling of the spin and kinetic temperatures.

The Ly α photons produced through X-ray ionization are “injected” photons, since they are introduced at the resonance line center. Spatial diffusion of these photons is negligible, because the width of the scattering line is much less than the Hubble expansion velocity of the Ly α sphere at the radius where the emission of these photons is important. To evaluate their intensity, we note that each X-ray will produce a number of Ly α photons $\eta_\alpha \nu / \nu_\alpha$, and that each Ly α photon produced in this way will have its frequency redshifted at a rate $H\nu_\alpha$ if the effect of scatterings are neglected, where H is the Hubble constant. Hence, the number density of these Ly α photons per unit of frequency should be equal to the heating rate per unit of volume (eq. 15) times the factor

$(\eta_\alpha/\eta)/(h\nu_\alpha)/(H\nu_\alpha)$. Their intensity is therefore equal to

$$J_i = \frac{c\eta_\alpha\Gamma}{4\pi h H \nu_\alpha^2}. \quad (17)$$

In terms of the fiducial intensity in eq. (5), we can rewrite this as

$$\frac{J_i}{\tilde{J}_0} = \frac{\eta_\alpha\Gamma}{\eta h \nu_\alpha n_H H}. \quad (18)$$

Noting that the quantity $h\nu_\alpha n_H H$ is roughly the heating rate required to heat the gas to a temperature $h\nu_\alpha/k_B \sim 10^5$ K over a Hubble time, we can easily see a relation between the temperature to which the gas is heated by X-rays and the Ly α intensity that can be produced from the same X-rays. For example, considering the gas temperature and Ly α intensity at half the lifetime of the star, $t = 1.5 \times 10^6 \text{yr} \simeq 10^{-2} H^{-1}$, at a distant point in the Ly α sphere where the temperature has been heated due to X-ray absorption by $\Delta T = 10$ K (still allowing for a large 21-cm absorption signal), and using $\eta_\alpha/\eta \simeq 4$ (valid for high neutral fractions and X-ray energies), an intensity $J_i/\tilde{J}_0 \simeq 4 \times 10^{-2}$ can be generated, sufficient to obtain $y_\alpha \simeq 2$ for the spin-kinetic temperature coupling.

We note here that the scattering of Ly α photons can also change the kinetic temperature of the gas. As shown by Chen & Miralda-Escudé (2004), the heating rate due to the Ly α scattering is negligible compared to that caused by X-rays, and we do not include it here. In fact, for the regime that we shall be interested here, the temperature of the atomic medium is high enough that the scattering of Ly α photons actually causes *cooling* of the gas (see Fig. 3 in Chen & Miralda-Escudé 2004), although by a negligible amount.

2.5. Results on the ionization and temperature profile evolution

We plot the neutral and ionization fraction of the gas as a function of distance from the star in Fig. 1, for a star of $200M_\odot$ at $z = 20$ and age 150 Myr. As can be seen from the figure, outside the HII region, the ionization fraction drops, but there is still some residue ionization, which is produced by the penetrating X-ray photons. At about 15 kpc, the ionization fraction approaches the background value. The spin and kinetic temperature

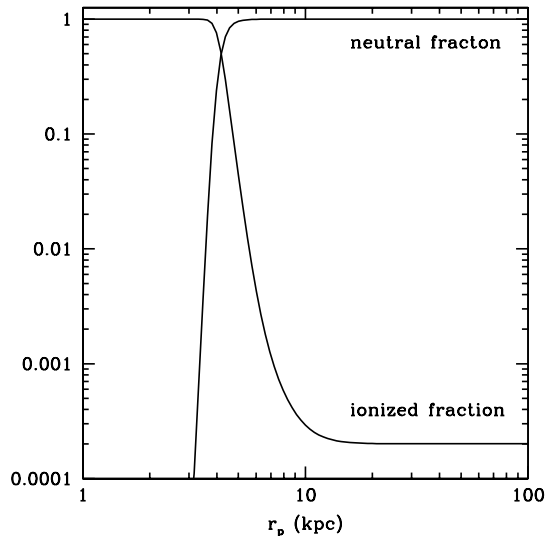


Fig. 1.— This shows the neutral and ionization fraction of H for a $200M_{\odot}$ star at $z = 20$, with age 1.5 Myr.

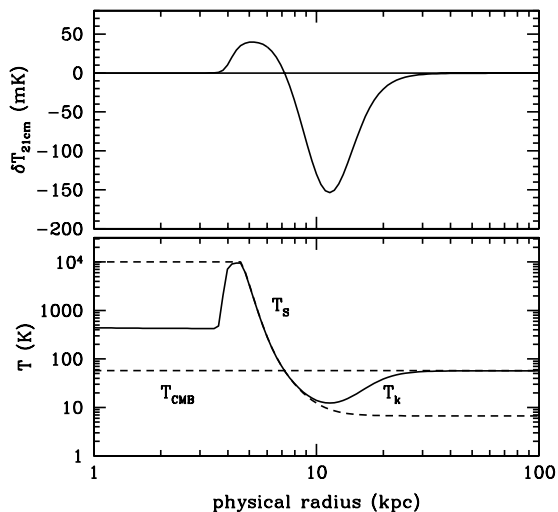


Fig. 2.— The kinetic and spin temperature (lower panel) and 21-cm brightness temperature (upper panel) of a first star (same condition as above).

profile, and the 21-cm brightness temperature is plotted in Fig. 2.

The spin temperature is strongly coupled to the kinetic temperature throughout the zone of the strong temperature drop ahead of the ionization front. The injected Ly α photons generated from the ionization by X-rays are far more intense than the continuum Ly α photons originating from the stellar photosphere. The y_{α} parameter (see eq. 3), which indicates how strongly the spin and kinetic temperatures are linked by the Ly α photons, becomes of order unity just at the radius where the atomic medium starts being heated above its initial temperature by the X-rays from the star (for the reason explained above in §2.4). At larger radius, the spin temperature gradually rises above the kinetic temperature towards the CMB temperature as the Ly α coupling becomes weaker. This produces a region of strong 21-cm absorption against the CMB, coming from the atomic medium that is starting to be ionized and heated, still far from the ionization front where most of the ionization occurs. The temperature in this region has not yet increased very much, allowing for a strong absorption signal, but the Ly α photons generated by the ionizations are already strong enough to lower the spin temperature by a large factor below the CMB temperature. Note that at very large radius, the spin temperature reaches a constant that is slightly below the CMB temperature because of collisional coupling, causing a constant level of absorption on the CMB.

Inside the HII region (the region that is mostly ionized), the kinetic temperature is assumed to stay constant. The spin temperature should also stay high, not only because of the Ly α photons produced by the high-energy electrons generated in the ionization front, but also because of additional Ly α photons generated by recombinations in the HII region. We have not calculated the detailed shape of the spin temperature profile in the HII region (this would be affected by diffusion of Ly α photons generated at the ionization front). However, this profile does not actually matter very much because, in the regime where the spin temperature is much higher than the CMB temperature, the observed 21-cm brightness depends only on the column density of hydrogen per unit of velocity, and not its spin temperature.

To see how these depends on the redshift, age,

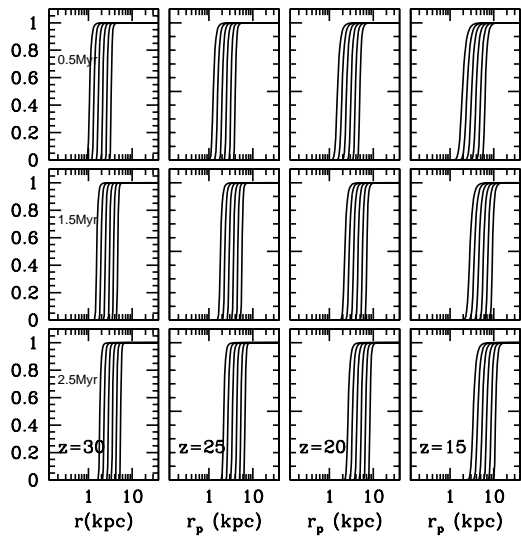


Fig. 3.— Neutral fraction as a function of radius in the HII region at the indicated redshifts and times after the birth of the star. In each panel, the six curves are for a star of mass $M = 25, 50, 100, 200, 400,$ and $800 M_{\odot}$, from bottom to top.

and mass of the star, we made plots of Fig. 3 and Fig. 4. In Fig. 3, the top, middle, and bottom panels correspond to a time after the birth of the star of 0.5, 1.5, and 2.5 Myr. The result is shown at redshifts $z = 30, 25, 20, 15$ from left to right. In each panel we plot the neutral fraction for six stellar masses: 25, 50, 100, 200, 400, and $800 M_{\odot}$. The ionized regions grow with the age of the star; for fixed stellar mass and age, the HII region is smaller at higher redshift because the gas is denser. The maximum physical radius reached is 1 to 10 kpc. The kinetic and spin temperatures of the Ly α sphere are plotted as a function of physical distance in the lower panels of Fig. 4, at a time $t = 1.5$ Myr and the four redshifts $z = 30, 25, 20,$ and 15. The six curves in each panel are for stellar masses $M = 25, 50, 100, 200, 400,$ and $800 M_{\odot}$. We have assumed that there is no global Ly α background or heating prior to the formation of the star. The kinetic temperature is equal to our imposed floor (10^4 K) within a few kiloparsecs, due to heating by ionization. Beyond this radius the kinetic temperature drops rapidly as the atomic zone is penetrated, until it reaches the

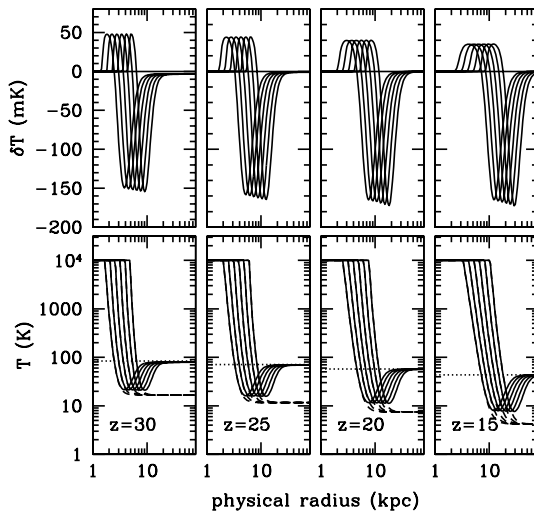


Fig. 4.— Brightness and temperature profiles of Ly α spheres, at a time $t = 1.5$ Myr and the indicated redshifts. *Bottom panels:* T_k (dash lines), T_{CMB} (dotted line), and T_S (solid lines). The six curves are for a star mass $M = 25, 50, 100, 200, 400,$ and $800 M_{\odot}$. *Top panel:* 21-cm brightness temperature fluctuation on the CMB at time $t = 1.5$ Myr.

constant value of the unheated atomic medium far from the star, which is below the CMB temperature owing to adiabatic cooling.

In Fig. 5, we plot the temperature profile if the Ly α photons are produced only from the star, and not by X-ray excitation. As can be seen from the figure, the coupling is much weaker so the spin temperature is not strongly coupled to the kinetic temperature, and the absorption signal is much weaker.

The Ly α sphere evolves as the gas is heated and ionized by the star. In Fig. 6, the same profiles are plotted at redshift $z = 20$ and three different ages, $t = 0.5, 1.5,$ and 2.5 Myr. The features of the Ly α sphere shift with time to larger radius and become shallower as the region where ionization and heating are important grows. A cross section map of the Ly α sphere for a star of $200 M_{\odot}$, age 1.5 Myr at $z = 20$ with no global heating is shown in the left panel of Fig. 17. The central HII region where $\delta T_b \simeq 0$, the emission region (red) and

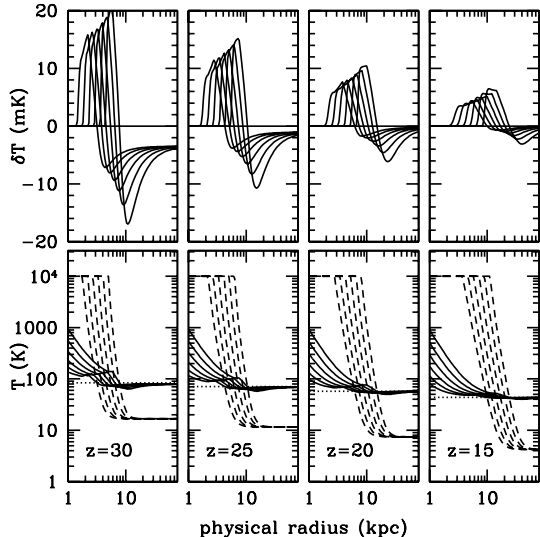


Fig. 5.— The temperature profile without X-ray induced photons.

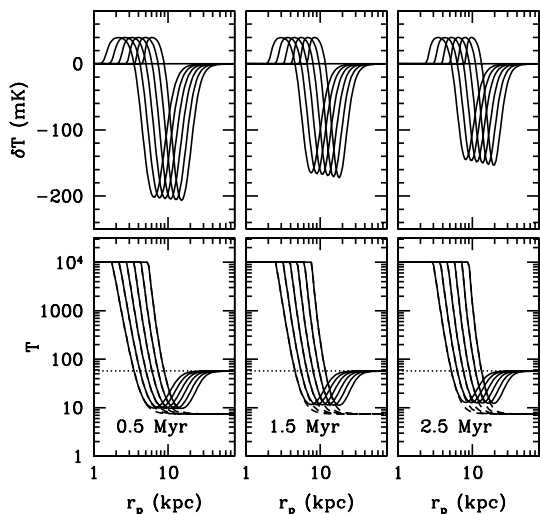


Fig. 6.— Brightness profile of Ly α spheres at $z = 20$, for the three indicated ages after the star birth.

absorption region (blue) is clearly seen. In real observations, the absorption signal against the CMB at large radius is the dominant signature of the Ly α sphere formed around a first star: it is of much higher brightness temperature and occupies a much larger area than the emission region close to the star that has been heated by the ionization. This small emission region could only be detected with very high angular and frequency resolution. In the absence of sufficient frequency resolution, the projected region of absorption on top of the small emission region would greatly overwhelm the signal.

3. Formation History

We now consider the formation history of the first stars in order to estimate the abundance of the Ly α spheres discussed in the previous section. We calculate the comoving density of collapsed dark matter halos with the halo model of Press-Schechter (Press & Schechter 1974), and also the Sheth-Tormen (Sheth & Tormen 1999) prescription. The density of collapsed halos of mass m at redshift z can be written as

$$N(m, z) = \frac{\rho}{m} s f(s) \frac{ds}{dm} \quad (19)$$

where $s = \delta_c^2(z)/\sigma^2(M)$, $\sigma(M)$ is the variance of the density fluctuation smoothed on a mass scale M with a top hat filter, and the critical linear overdensity is $\delta_c(z) = 1.686/D(z)$, where $D(z)$ is the linear growth factor. The function $f(s)$ is

$$s f(s) = A \left(1 + \frac{1}{s^p}\right) \sqrt{\frac{s'}{2\pi}} e^{-s'/2}. \quad (20)$$

Here, $s' = as$, with $A = 1/2$, $a = 1$, $p = 0$ for the Press-Schechter (PS) mass function, and $A = 0.322$, $a = 0.707$, $p = 0.3$ for the Sheth-Tormen (ST) mass functions.

The gas in a dark matter halo can form a first star provided that the primordial gas in the halo is able to cool by means of the small fraction of molecular hydrogen that can be made at this early epoch, faster than the rate at which the gas is dynamically shock-heated during mergers and accretion (e.g., Yoshida et al. (2003), Reed et al. (2005)). We assume for simplicity that star formation proceeds in any halo with $T_{\text{vir}} > 2000\text{K}$, where T_{vir} is the gas temperature after virialization and in hydrostatic equilibrium. For neutral

gas, the mass of the halo when the virial temperature reaches this value is

$$M_{min}(z) = 1.17 \times 10^6 \left(\frac{\Omega_m h^2}{0.147} \right)^{-1/2} \times \left[\frac{(1+z)}{21} \right]^{-3/2} \frac{T_{vir}}{2000\text{K}}. \quad (21)$$

The lifetime of one of these massive, first stars is $t_* \approx 3\text{Myr}$, so only halos that have formed within the last t_* would possess an active star. We assume here that only one metal-free star forms per halo, since the ionizing radiation from these massive stars is able to ionize and expel all the gas in the halo (e.g., Whalen, Abel, & Norman (2004)), and any future stars will already form from metal-enriched gas (presumably with a mass function closer to the present one).

After its main sequence life time, a first star may explode as a supernova and destroy itself completely; or explode as a supernova and left behind a black hole or neutron star; or collapse into a black hole directly (Woosley, Heger, & Weaver 2002). In the absence of continued supply of X-ray and Ly α photons, the Ly α sphere dims as the scattering Ly α photons diffuse out. However, supernovae remnant and accreting black hole may become new source of light, the Ly α sphere could be maintained, or even grow to much larger size. We will investigate these interesting possibilities in subsequent work.

For simplicity, we assume that one star is present in each halo that has just formed with mass $M > M_{min}(z)$. At high redshift, when the fraction of matter that has collapsed in halos in which gas can cool is small, the number of halos of mass m that have formed over a time t_* can be approximated as

$$n_* = \int_z^{z_a} dz \int_{M_{min}(z)}^{\infty} dm \frac{\partial N(m, z)}{\partial z}, \quad (22)$$

where the cosmic time at z_a is $t(z_a) = t(z) - t_*$. In the redshift range $15 \lesssim z \lesssim 40$, this can be simplified as

$$n_* \approx (1+z)H(z)t_* \int_{M_{min}(z)}^{\infty} dm \frac{\partial N(m, z)}{\partial z} \quad (23)$$

At low redshift, the approximation obviously fails as halo destruction by mergers becomes important. At high redshift $n(m, z)$ evolves too rapidly

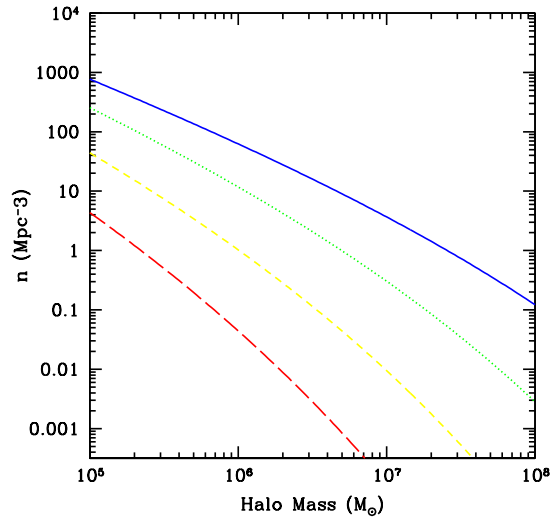


Fig. 7.— Number density of star-harboring halos of mass m per comoving Mpc^{-3} per $\log m$. The four curves are at $z = 15$ (solid, blue curve), $z = 20$ (dotted green curve), $z = 25$ (short-dash yellow curve), and $z = 30$ (long-dash red curve).

and the integration over redshift needs to be done more carefully.

We plot the mass function of halos formed within a time t_* , calculated with the Press-Schechter formalism in Figure 7. In Figure 8, the comoving densities of star forming halos (solid curves) and first stars (dashed curve; this is equal to the density of halos formed within the past three million years) are shown, both for the Press-Schechter and Sheth-Tormen mass functions. The ST mass function predicts a higher abundance for rare fluctuations, so at very high redshift the ST result is substantially greater than the PS result. At lower redshifts the ST function fits N-body simulation results better, although it tends to over-predict the number of halos at $z > 10$ (Reed et al. 2003). The accuracy of the mass functions at such high redshifts is still largely unknown, different conclusions were reached in different numerical studies (Jang-Condell & Hernquist 2001; Jenkins et al. 2001; Reed et al. 2003; Iliev et al. 2006; Zahn et al. 2006; Warren et al. 2006; Lukic et al. 2007), and in fact may also depend on the definition of the halo and its mass in the simulation (Cohn & White

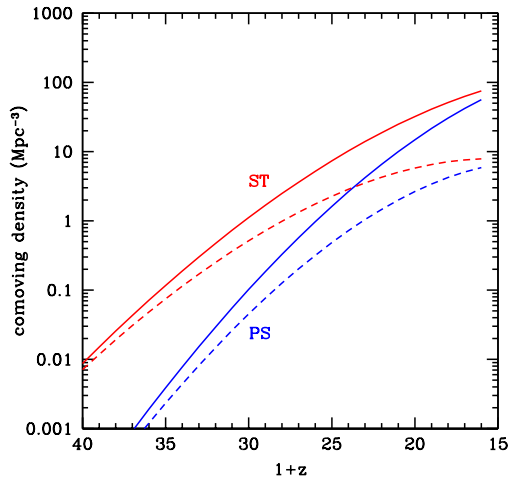


Fig. 8.— Comoving density of halos and first stars. *Solid curves*: total density of star-forming halos. *Dashed curves*: density of star-forming halos formed in the past 3 Myr. Results are shown for the Press-Schechter (PS) and Sheth-Tormen (ST) halo mass functions.

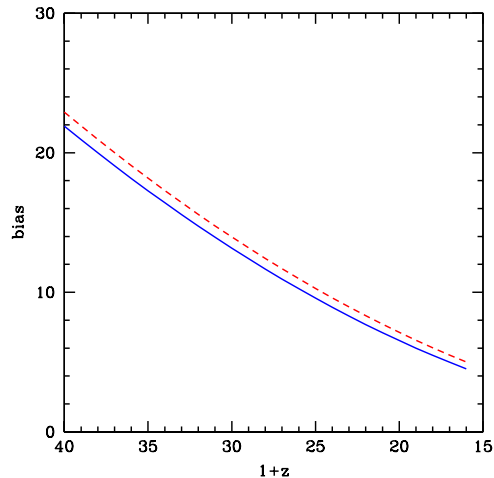


Fig. 9.— Bias factor of star-forming halos for the PS function (solid curve) and ST function (dashed curve).

2007).

The comoving density of first stars peaks around a redshift $z \sim 15$. Our calculation begins to fail at this redshift for several reasons: the merger destruction rate of the halos becomes comparable to the formation rate, and equation 22 is no longer accurate. Physical feedback effects suppressing the formation of metal-free stars and new star formation in regions containing metals may become important even earlier than $z = 15$. We do not consider these uncertainties in this paper, where we merely want to illustrate how the Ly α spheres of the first stars may interact, so our calculation is stopped at $z = 15$.

Halos harboring the first stars are strongly clustered because of the flatness of the Cold Dark Matter power spectrum at small scales, which implies a high bias of the first objects in large-scale regions of high density. The bias of halos of mass M at redshift z can be approximated as (Mo & White 1996, 2002)

$$b = 1 + \frac{s(M, z) - 1}{\delta_c(0)} \quad (24)$$

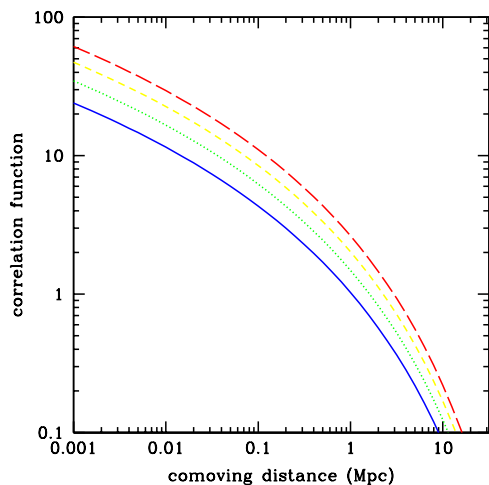


Fig. 10.— Correlation function of star-forming halos, at redshifts $z = 15, 20, 25,$ and 30 (from bottom up), calculated with the Press-Schechter function. Note that the correlation function increases with redshift, because of the increasing bias factor.

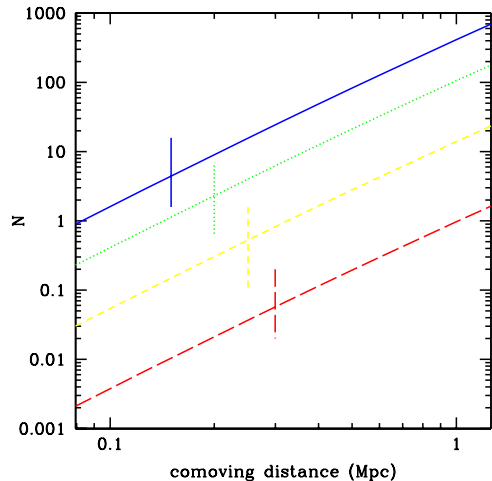


Fig. 11.— Expected number of star-forming halos as a function of distance. The four curves are $z = 15$ (solid, blue curve), $z = 20$ (dotted green curve), $z = 25$ (short-dash yellow curve), and $z = 30$ (long-dash red curve). A physical distance of 10 kpc (the approximate size of the Ly α spheres) is marked at each redshift.

for the PS function, and

$$b = 1 + \frac{1}{\delta_c(0)} \left[s' + 0.5s'^{0.4} - \frac{s'^{0.6}/0.84}{s'^{0.6} + 0.14} \right] \quad (25)$$

for the ST function. We calculate the bias corresponding to the minimal mass for halos harboring stars at each redshift. The result is shown in Fig. 9. The bias grows very rapidly with redshift, faster than $(1+z)$, implying that (perhaps counter-intuitively) the first stars are increasingly clustered as the redshift increases, at a fixed comoving scale.

The correlation function of biased halos is given by

$$\xi_{hh}(r, z) \approx b^2 \xi_{lin}(r, z), \quad (26)$$

where the linear correlation function is

$$\xi(r, z) = \int \frac{d^3k}{(2\pi)^3} P_{lin}(k, z) e^{ikr}. \quad (27)$$

We plot the correlation functions in Fig. 10. The increasing amplitude of the correlation function with redshift is again a result of increasing bias factor with redshift.

The average number of neighboring Ly α spheres within a given radius r is (neglecting higher order clustering terms)

$$\bar{N}(R) = \bar{n}(z) \int_0^R d^3r [1 + \xi(r)], \quad (28)$$

where $\bar{n}(z)$ is the number density of star forming halos. Note that this calculation is not very accurate, as non-linear effect may be important at such small scales, it is only meant to give an idea on how the Ly α spheres are correlated. The result is shown in Fig. 11. The average number of halos within a sphere of physical radius $r = 10$ kpc is ~ 0.04 at $z = 30$ and ~ 4 at $z = 15$. This number increases with time because of the growing number of collapsed halos, despite the decrease in the correlation function. Even if several similar halos are found within the radius of the Ly α sphere, the formation time of the two stars may not coincide, thus the observed density of Ly α sphere is $f_* \bar{N}$, where the duty cycle factor $f_* \sim n_*/n_{halo} < 1$. Moreover, feedback effects (e.g., from molecular photodissociation) of the radiation of one star may adversely affect the formation of the other one.

The large biasing factor of the star-harboring halos implies that the first stars which produced Ly α spheres may have an irregular neighborhood, with more collapsed structures on the scale of the Ly α sphere than one would find in a random location of the universe. These density fluctuations will likely make the “Ly α spheres” have a structure that is not actually very spherical, but irregular.

4. The impact of Ly α and hard X-ray backgrounds

4.1. The Ly α background

In §2, we have computed the kinetic and spin temperature profiles of the atomic medium around an isolated first star. The largest signal this “Ly α sphere” produces in 21-cm is the absorption against the CMB at large distances from the star. This absorption can be detected against the background if the spin temperature of the atomic medium is coupled to the kinetic temperature only close to the star, but not far from it because of the absence of Ly α photons; each star would then produce an isolated Ly α sphere. However, as the number of first stars increases, a Ly α background

will be generated which can couple the spin and kinetic temperatures everywhere, producing a global absorption signal against which the regions near one star would be harder to detect. In fact, owing to the presence of the foreground, it is not possible to make absolute measurements of the 21-cm signal, but only its spatial variations and non-smooth variation in redshift. In Figures 4 and 17, the plotted emission (absorption) temperature is not the absolute value, but the difference its value far from any Ly α sphere.

The Ly α background originates from the continuum photons emitted by the stellar photospheres. This is because the injected photons resulting from the high-energy electrons generated by soft X-ray photons are emitted at the Ly α line, and are rapidly redshifted as they leave the Ly α sphere where they have been created. On the other hand, hard X-ray photons may penetrate the Ly α sphere and produce some injected photons very far from the sources, but the total energy released in hard X-ray photons by the first stars is less than that in UV photons, and only a very small fraction of the hard X-ray photon is absorbed in the IGM to produce injected Ly α photons. Because the injected photons vastly dominate the intensity over the continuum photons from the central star, the background of Ly α photons is much fainter than it would be if continuum photons were the dominant ones. This allows for a lasting contrast of individual Ly α spheres in comparison to the background, because the Ly α background intensity stays low even when a very large number of first stars are seen from any random point in the universe.

At the same time, we need to take into account the background of X-rays produced by the stars and their global heating effect, which will raise the kinetic and spin temperatures and hence decrease the strength of the 21-cm absorption.

To compute the background of the continuum photons near the Ly α line, we assume a blackbody spectrum for the first stars. Let $E(\nu)$ be the number of photons emitted over all time per baryon and per unit of frequency in one of the halos that collapse to form the first stars. In a halo that forms a single, massive metal-free first star, the spectrum should be a blackbody with temperature $T \simeq 10^5$ K, with little dependence on the stellar mass (Schaerer 2002). As more massive halos collapse and continue to form stars from metal-

polluted gas, different stellar populations should form and emit more photons. For simplicity, we shall assume here that $E(\nu)$ remains constant, that is to say, the total number and spectrum of photons emitted per baryon in collapsed halos is fixed at frequencies greater than Ly α (which are the only ones that affect our result). In view of our present ignorance on the type of stars that will form in halos of different mass as the processes of collapse of structure in the universe, reionization and metal pollution proceed, this assumption seems as good as any other.

The fraction of mass bound in star-forming halos is

$$F(z) = \int_{M_{\min}(z)}^{\infty} m \frac{dN(m, z)}{dm} dm, \quad (29)$$

where $\frac{dN(m, z)}{dm}$ is the comoving density of halos of mass m , and $M_{\min}(z)$ is the minimum halo mass to form the first stars at redshift z . The star formation time and the main-sequence lifetime of the first stars are short compared to the Hubble time, so the emissivity can be approximately written as

$$\epsilon(\nu, z) = n_H E(\nu) \dot{F}. \quad (30)$$

where \dot{F} is the time derivative of the fraction of mass bound in star-forming halos, F , and we have assumed a constant $E(\nu)$.

As mentioned above, the only photons that contribute to the Ly α background are those emitted by the stars in the continuum to the blue of the Ly α line. Among these, only photons with $\nu < \nu_\beta$ can be redshifted to ν_α as continuum photons, and all photons of greater frequency will be absorbed at the Lyman β or higher resonance Lyman series lines and be converted to injected Ly α photons. Here we will calculate only the intensity of the continuum Ly α background, and we will need to bear in mind that the total background will actually be a little bit larger because of the injected photons from higher Lyman series lines (note that the spin changes caused by these higher Lyman series photons before they convert to Ly α photons are negligible, because of the very large number of scatterings that the Ly α photons undergo). This intensity is given by

$$\frac{J}{\tilde{J}_0} = E_\alpha \nu_\alpha \int_z^{z_\beta} \frac{dF(z')}{dz'} E \left[\frac{1+z'}{1+z} \nu_\alpha \right] / E_\alpha dz', \quad (31)$$

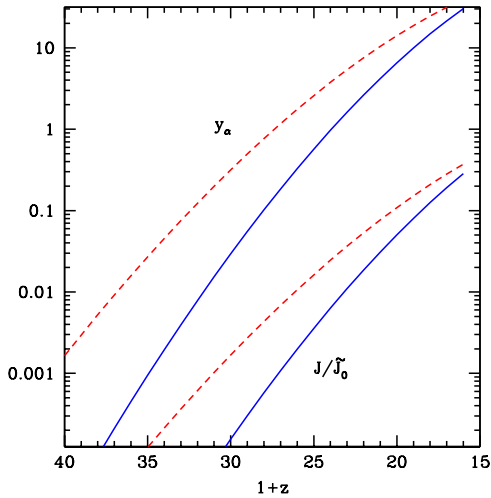


Fig. 12.— Ratio J/\tilde{J}_0 (lower curves) and y_α (upper curves) as a function of redshift. Solid curves are for the Press-Schechter mass function, dashed curves are for the Sheth-Tormen mass function.

where $E_\alpha = E(\nu_\alpha)$. If the spectrum of first stars $E(\nu)$ is approximated as flat near the Ly α frequency (which is a good approximation for massive, metal-free stars, which have surface temperature of 10^5 K), then the expression is simplified to

$$\frac{J}{\tilde{J}_0} = E_\alpha \nu_\alpha [F(z) - F(z_\beta)]. \quad (32)$$

We obtain an estimate for the value of E_α as follows: a typical halo with baryonic mass of $10^5 M_\odot$ forming one star with $10^2 M_\odot$ uses a fraction 10^{-3} of its mass to form stars. If $\sim 50\%$ of this mass is hydrogen that is burned to helium in the stellar interior during the star lifetime, the energy released per baryon in the halo is $e_b = 7 \text{ MeV} \times 10^{-3} \times 0.5 = 3.5 \text{ keV}$. Assuming a blackbody spectrum with photospheric temperature T , we find

$$E_\alpha \nu_\alpha = \frac{15}{\pi^4} \frac{1}{\exp(h\nu_\alpha/kT) - 1} \left(\frac{h\nu_\alpha}{kT} \right)^4 \frac{e_b}{h\nu_\alpha}. \quad (33)$$

For $T = 10^5$ K, this expression gives $E_\alpha \nu_\alpha \simeq 45$. We use this value to compute the background intensity.

The fraction of mass bound in halos above the minimum mass to form stars is computed for the two halo models we use, i.e., the Press & Schechter

(1974) model,

$$F = \text{erfc}(\sqrt{s/2}), \quad (34)$$

and the Sheth & Tormen (1999) model,

$$F = 0.4 \left[1 + \frac{0.4}{s^{0.2}} \text{erfc}(0.85\sqrt{s/2}) \right], \quad (35)$$

where $s = \delta_c^2(z)/\sigma^2(M_{min})$. The resulting Ly α intensity is plotted as a function of z in Figure 12. The corresponding y_α , which gives the strength of the spin-kinetic coupling by Ly α scattering, is also shown in the same figure.

The figure shows the Ly α background intensity becomes important at very high redshift. For the Sheth-Tormen model, $y_\alpha > 1$ at $z < 28$, while for the Press-Schechter model, this is only slightly delayed (at $z = 25$).

It may seem surprising that the background becomes important at such an early stage in the formation of the first generation of stars, because as mentioned earlier the flux of local Ly α photons in a Ly α sphere is actually dominated by the secondary Ly α photons produced from the ionization by X-rays, whereas the Ly α background is contributed only by the direct ultraviolet emission from the distant stars. But this is compensated for by the large number of first stars that are already visible from any location out to a large distance in the universe at these redshifts. This can be seen considering, as an illustration, that each star in the universe emits a luminosity L_i in X-rays that are absorbed at radius $\sim r_\alpha$ and have their energy converted into “injected” Ly α photons, and a luminosity L_c of “continuum” photons in each frequency range $\Delta\nu/\nu_\alpha = Hr_\alpha/c$, which enter the resonance Ly α line as they propagate through a distance equal to the size of the Ly α sphere. Then, the local flux of Ly α photons from the star (dominated by the injected ones) is $F_i = L_i/(4\pi r_\alpha^2)$, and the background flux (determined by the continuum photons) is $F_b = n_\alpha L_c r_m$, where n_α is the number density of Ly α spheres with first stars of similar luminosity, and r_m is the maximum distance out to which these first stars can be seen. In practice, r_m is determined by the extremely fast evolution of the density of first stars (which parallels that of the background intensity shown in Fig. 12), which doubles every $\Delta z \simeq 2$. Hence, $r_m \sim cH^{-1}\Delta z/(1+z)$. Defining the filling factor

of the Ly α spheres $f = 4\pi n_\alpha r_\alpha^3/3$, we find that

$$\frac{F_i}{F_b} = \frac{L_i}{L_c} \frac{r_\alpha}{r_m} \frac{1}{3f}. \quad (36)$$

For the first stars at $z \sim 30$ and at $r_\alpha = 10$ kpc, $L_i/L_c \sim 100$ (as determined from a blackbody spectrum with $T \simeq 10^5$ K), and $r_m/r_\alpha \sim 300$, so the background of continuum photons becomes equal to the locally produced injected photons when the filling factor of the Ly α spheres is about 10%. The fluctuation in Ly α photon flux as a function of smoothing scale was also discussed by Barkana & Loeb (2005a).

Hence, the background starts diminishing the contrast of the Ly α spheres when their filling factor becomes large. Of course, when the filling factor becomes large the background of injected Ly α photons generated by X-rays from other stars (which we have not included here) should also become important. The importance of other stars in the neighborhood is greatly increased by the large biasing of the first stars. As we can see in Fig. 11, we typically expect to find several other halos capable of forming metal-free stars within the distance of the physical size of the Ly α sphere (~ 10 kpc) at $z \lesssim 25$. This means that in practice, at $z \lesssim 25$ some of the Ly α spheres may actually be produced by ‘‘clusters’’ of first stars, where several stars contribute to the Ly α fluxes of large blobs yielding 21-cm absorption.

4.2. The X-ray background

In addition to the soft X-rays from the stellar photosphere, the intergalactic medium may also be heated up by a hard X-ray background, produced for example by a population of early X-ray binaries after some of the metal-free stars have collapsed into black holes, or by supernova explosions and the relativistic electrons generated in supernova remnants. The hard X-rays heat the atomic medium globally, because their mean free path is large compared to the typical separation between Ly α spheres (as opposed to the soft X-rays from the metal-free main-sequence stars, which do not heat the medium substantially beyond the radius of a Ly α sphere as discussed in §2). For local star bursts, it has been estimated that the energy release in hard X-rays is (Oh 2001)

$$L_X \sim 5 \times 10^{40} \text{erg} \frac{\text{SFR}}{M_\odot \text{yr}^{-1}} \quad (37)$$

or about $\epsilon_X \sim 1$ keV per baryon that forms stars. At high redshift the X-ray emission may increase because of the higher temperature of the CMB which provides seed photons for Compton scattering (Cen 2003).

In practice, only a small fraction of the energy emitted in hard X-rays will be used to heat the IGM. At very high frequency, the universe is transparent to X-ray photons and so most of the emitted energy will be redshifted rather than absorbed by an atom. At redshift $z = 30$, the universe is opaque below a photon energy of ~ 2 keV. Only a small fraction of the energy of the absorbed photons will be converted to heat (the rest being used for collisional ionizations and excitations). If η_{eff} is the fraction of the emitted X-ray energy converted to heat, and f_* is the fraction of baryons in collapsed halos with $M > M_{min}(z)$ that form stars, then the temperature evolution of the gas is described by (neglecting other heating and cooling mechanisms such as shock heating, Compton effect, etc.)

$$\frac{dT}{dz} = -F \frac{f_* \eta_{eff} \epsilon_X}{\mu k_B} + \frac{2T}{1+z}. \quad (38)$$

To see a characteristic example for the gas temperature evolution, we integrate this equation using $f_* \eta_{eff} = 2 \times 10^{-5}$ (a reasonable value obtained for $f_* \sim 2 \times 10^{-3}$ for a typical metal-free star formed in a halo with $\sim 10^5 M_\odot$ of baryons, and a fraction $\eta_{eff} \sim 10^{-2}$ if 10% of the hard X-ray energy is emitted in the relevant range 0.2–2 keV and 10% of this energy is converted into heat). We start at $z = 60$ with a mean gas temperature of 66.6 K as given by the code RECFAST (Seager, Sasselov & Scott 2000). The results are shown in Fig. 13. The CMB temperature and the adiabatically evolved gas temperature are also shown. The evolution of the mean temperature of the IGM depends sensitively on the hard X-ray emission. For $\epsilon_X \sim 1$ keV per baryon, the mean gas kinetic temperature is below that of the CMB down to $z \sim 11$, but for $\epsilon_X \sim 10$ keV, the gas is heated above the CMB temperature at $z \sim 15$ –17 in our model.

We plot the profiles of the Ly α sphere in the presence of hard X-ray heating in Fig. 14, with $\epsilon_X = 10$ keV per baryon, $f_* \eta_{eff} = 2 \times 10^{-5}$, and using PS halo model. At high redshift ($z = 30$ to 25), when X-ray heating is still not significant,

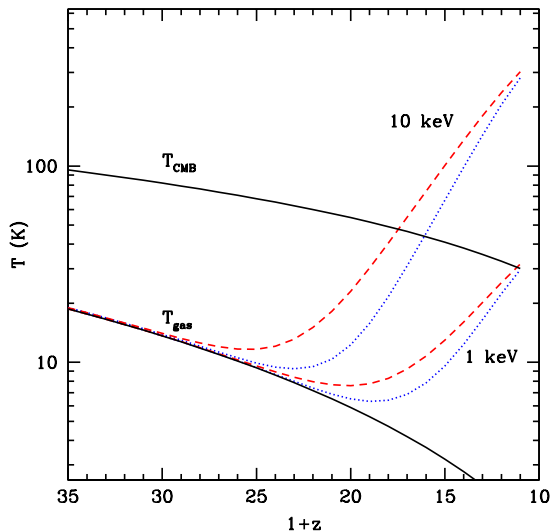


Fig. 13.— Temperature evolution of the IGM. Solid curves show T_{CMB} and the adiabatically evolved gas temperature. Short and long-dash curves show the IGM heated by X-rays, with the PS (short dash) and ST (long dash) model calculations. Two sets of curves are plotted, for $\epsilon = 1$ keV and 10 keV respectively.

the profiles are similar to those shown in Fig. 4. At lower redshifts, however, the gas is gradually heated and therefore the 21-cm absorption becomes gradually weaker. For $\epsilon = 10$ keV, the Ly α sphere would of course appear in emission everywhere for $z \lesssim 20$ because the gas kinetic temperature is globally heated above the CMB temperature (see the right hand panel of Fig 17, which shows a $200 M_{\odot}$ star at $z = 15$ where the mean temperature of the gas is already heated above the CMB temperature).

It needs to be born in mind that the history of heating of the IGM is completely dependent on the type of X-ray sources that appeared among the first population of stars. These are likely to be X-ray binaries made by the first stellar black holes, in stars that are formed as close binaries. It is also possible that a population of miniquasars made when gas can cool in the vicinity of these first black holes emitted X-rays efficiently. The parameters we have chosen here for the X-ray emission should be considered as no more than an il-

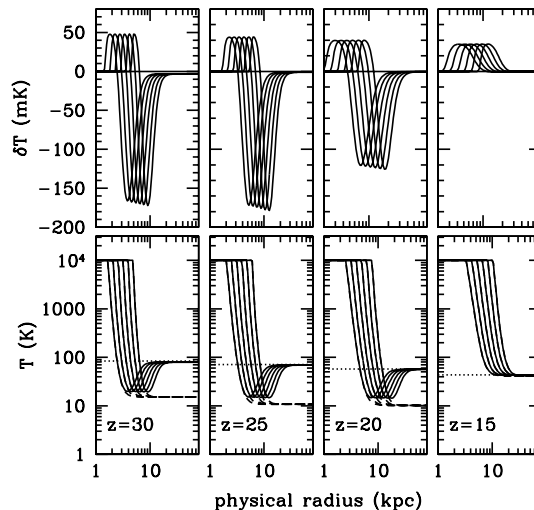


Fig. 14.— Brightness and temperature profiles of Ly α spheres, as in Fig. 4 except with X-ray heating of 10 keV per baryon.

lustrating example, because we cannot predict the abundance of these first X-ray sources. The possibility of observing the transition from Ly α spheres with a strong absorption signal to a weaker emission signal at lower redshift would provide a very useful tool to study the thermal evolution of the atomic IGM and the nature of the first sources in the universe.

Our simple estimate of the Ly α and X-ray background are in general agreement with other analytical models, e.g. Sethi (2005); Furlanetto (2006). However, Sethi (2005) noted that the the actual process of X-ray heating may be an inhomogeneous one. Some part of the IGM gas would be heated earlier and to higher temperature than other parts. With such temperature variations, one would observe that for the same redshift, some Ly α spheres have only weak emission signal, while others have strong absorption signal. Observation of such phenomena would reveal the temperature variations of the IGM (see also Pritchard & Furlanetto 2007).

5. Observability

So far we have presented a theoretical investigation of the properties of what we have named “Ly α spheres”, the first regions of the universe illuminated by Ly α photons from a metal-free star or a “cluster” of such stars (where the clusters would be caused by biasing in the cosmological distribution of star-forming halos). Would it be possible to observe this object directly with the incoming 21-cm instruments, such as 21CMA/PAST, LOFAR, MWA, and SKA? Or, if not these instruments, can we design one which could do it? What would be the characteristics of an instrument optimized for detecting the Ly α sphere of the first stars?

If the instrument has a response function $R(\nu, \vec{\theta})$, with $\int d\nu d\theta^2 R(\nu, \vec{\theta}) = 1$, then for a pixel centered on the Ly α sphere, the resulting signal is

$$\hat{T} = \int d\nu d\theta^2 R(\nu, \vec{\theta}) \delta T(\nu, \vec{\theta}). \quad (39)$$

We can model $R(\nu, \vec{\theta})$ as a direct product of a top-hat spectral function with a bandwidth $\Delta\nu$ and a Gaussian beam of half-beam width Θ . Then,

$$\delta\hat{T} = \frac{1}{2\pi\Theta^2\Delta\nu} \int_{\nu(z)-\frac{\Delta\nu}{2}}^{\nu(z)+\frac{\Delta\nu}{2}} d\nu \int_0^\infty d^2\theta \delta T(\nu, \vec{\theta}) e^{-\theta^2/2\Theta^2}. \quad (40)$$

For an interferometer array, the real space pixel noise is given by (Thompson, Moran, & Swenson 2001; Santos, Cooray & Knox 2004)

$$\Delta T \sim \frac{T_{sys}}{f_{cov}\sqrt{\delta\nu t}}, \quad (41)$$

where T_{sys} is the system temperature, $\delta\nu$ is bandwidth, t the observation time, and

$$f_{cov} = N_{dish} A_{dish} / A_{total} \quad (42)$$

is the covering factor of the array. Here, A_{dish} is the area of an antenna, and A_{total} is the total area of the square made by the base line of the array. The angular resolution of the array is

$$\Theta \sim \left(\frac{A_{dish}}{A_{total}} \right)^{1/2} \sim \frac{\lambda}{L}, \quad (43)$$

where L is the baseline, and λ the redshifted wavelength. Thus, for a fixed value of $N_{dish} A_{dish}$, the

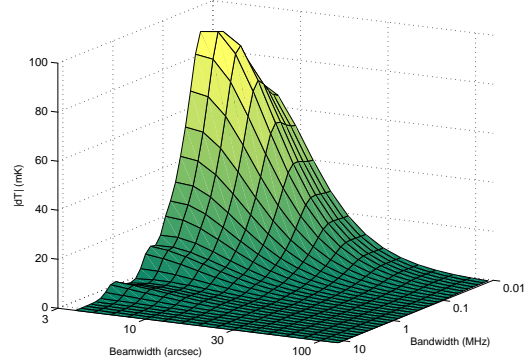


Fig. 15.— The absolute value of the signal $|\delta\hat{T}|$ as a function of beamwidth Θ and bandwidth $\Delta\nu$, for a star at $z = 20$, with a mass of $400 M_\odot$ and an age of 1.5 Myr.

covering factor decreases with resolution. The signal to noise ratio of the measured radio brightness within a resolution element of the array is

$$\text{SNR} = \sqrt{\Delta\nu t} f_{cov} \frac{\delta\hat{T}}{T_{sys}}. \quad (44)$$

The system temperature is dominated by the galactic synchrotron background, which scales as $\nu^{-2.5}$, or in terms of redshift,

$$T_{sys} \simeq 2000\text{K} \left(\frac{1+z}{21} \right)^{2.5}. \quad (45)$$

The signal to noise ratio at redshift z is then

$$\text{SNR} \sim 3f_{cov} \left(\frac{1+z}{21} \right)^{-2.5} \left(\frac{\Delta\nu \cdot t}{10 \text{ kHz} \cdot \text{yr}} \right)^{1/2} \left(\frac{\delta T}{10 \text{ mK}} \right). \quad (46)$$

At redshift z , and for a flat space geometry, a comoving distance dr is related to angular size $d\theta$ and frequency variation $d\nu$ by

$$d\theta = dr/r, \quad d\nu = \nu_0 \frac{H dr}{c(1+z)^2}, \quad (47)$$

where $r = \int c dz/H$. The comoving distance is related to the physical distance by $r = (1+z)r_p$. For the Ly α spheres, the relevant physical scale is ~ 10 kpc. For the set of cosmological parameters adopted by us, a physical distance of 10 kpc at

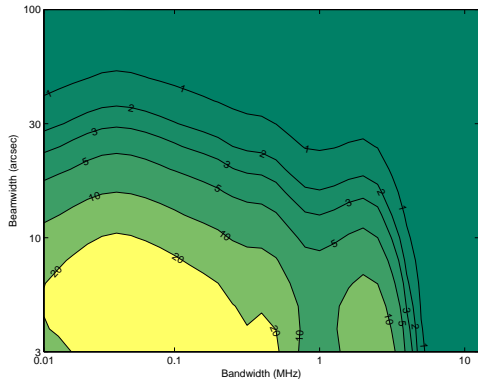


Fig. 16.— The signal to noise ratio SNR as a function of beamwidth Θ and bandwidth $\Delta\nu$, for a star at $z = 20$, with a mass of $400 M_{\odot}$ and an age of 1.5 Myr, assuming $f_{cov} = 1$ and $t = 1\text{yr}$.

redshift $z = 20, 30$ corresponds to an angular scale of 3.9, 5.3 arcsec and a frequency interval of 7.6, 9.2 kHz, respectively.

In a resolved observation, the maximum absorption signal strength can reach a value close to $\delta T \sim -200\text{mK}$ (Fig. 4). However, in order to resolve the Ly α sphere, a beam of $\Theta \lesssim 4''$ and frequency bandwidth $\nu \lesssim 8\text{kHz}$ are required. For observations of the redshifted 21-cm line, the baseline for achieving an angular resolution θ is given by

$$L = 910 \left(\frac{1+z}{21} \right) \left(\frac{\theta}{1''} \right)^{-1} \text{ km} . \quad (48)$$

For a beamwidth and bandwidth similar to the size of the Ly α sphere, one obtains the best signal-to-noise ratio for a single brightness measurement. Assuming that the center of the beam and frequency bin is centered on the star, we plot the observational signal $|\delta\hat{T}|$ of the Ly α sphere made by a $400M_{\odot}$ star at $z = 20$ of age $t = 1.5\text{Myr}$, as a function of the beamwidth Θ and bandwidth $\Delta\nu$ in Fig. 15. For this star, the maximum emission brightness occurs at 6.9 kpc away from the star, and the maximum absorption is located at 15 kpc ($\delta T = -190\text{mK}$), but $|\delta T| > 5\text{mK}$ up to 33 kpc. The signal decreases more rapidly with Θ than $\Delta\nu$, which is not unexpected given that the included volume is $\propto \Theta^2 \Delta\nu$. There are some wiggles of δT in the $\Delta\nu$ direction, probably because

as we vary the size of the frequency window, we are sampling different structure of the Ly α sphere.

We plot the corresponding signal to noise ratio (SNR; see eq. [46]) in Figure 16, assuming $f_{cov} = 1$ and $t = 1\text{yr}$. Again, we ignore the second peak at very large bandwidth. To obtain a high confidence detection with $\text{SNR} > 5(10, 20)$ under this circumstance, one could choose an optimal bandwidth of 30 kHz, and the optimal beamwidth (to obtain the highest SNR) is 20 (14, 10) arcsec, corresponding to a baseline of 45 (65, 91) km. The area corresponding to this baseline would have to be covered with dipole receivers in order to achieve $f_{cov} \sim 1$. The requirements become more stringent with increasing redshift, owing to the increasing brightness of the synchrotron foreground, and as we have seen in §4 it may be necessary to go up to $z \sim 30$ to see a pristine Ly α sphere with a signal that is not yet weakened by a global Ly α background and an IGM heated by hard X-rays.

6. Conclusion

We have investigated the 21-cm signature of the first stars. The coupling of the spin and kinetic temperature induced by the Ly α photons generated by a metal-free star should generate a “Ly α sphere”, a region that can be detected by a 21-cm absorption signal when the IGM has not been heated by X-rays prior to the formation of the star. The 21-cm absorption signal can reach a strength of 200 mK when the IGM temperature far from the star is at its minimum value reached by the adiabatic cooling, and becomes weaker as the IGM is heated. Most of the Ly α photons that couple the spin and kinetic temperatures are generated by collisional excitations of the high-energy electrons that are produced by soft X-rays emitted from the photospheres of the hot metal-free stars, rather than the direct photospheric emission of the star. These soft X-rays are not able to travel very far from the star and hence tend to heat the IGM only locally around each metal-free star that forms, but the IGM may be heated globally by other sources of hard X-rays, such as X-ray binaries formed by the black holes made by the first stars.

The temperature and 21-cm absorption profile of a Ly α sphere can be calculated as a function of the spectrum emitted by the star and its age in the idealized case of a uniform medium in Hub-

ble expansion around the star. However, owing to the highly biased distribution of the first stars, the region where a first star has formed may often be highly irregular, containing non-linear structures on scales larger than the halo hosting the star. The first stars should also be highly clustered because of their biased distribution, so the high-redshift regions producing 21-cm absorption may often be produced by several first stars that are illuminating and heating a larger region with their X-rays and Ly α photons. This may make these regions larger and therefore easier to detect.

The detection of these earliest structures in the universe formed by the first stars is still very challenging, mainly because of the high redshift at which they are likely to be present and the intense synchrotron foreground that must be subtracted to measure any CMB fluctuations. Filled aperture of at least ~ 50 km will be required for detection³. However, detecting these regions of Ly α absorption will represent a milestone for cosmology: they will constitute a clear indication that the first stars formed in the universe have been found, and allow us to measure many of their properties such as their mass distribution and spatial correlation.

We thank Chris Hirata, Steven Furlanetto, Ue-Li Pen, Pengjie Zhang, and the anonymous referee for discussions and suggestions. XC acknowledges the ICRA and the Caltech TAPIR group for their hospitality during his visit. XC is supported by the NSFC under the Distinguished Young Scholar grant No. 10525314, the Key Project grant No. 10533010, by the CAS under grant KJCX3-SYW-N2, and by the Ministry of Science of Technology under the National Basic Science Program (Project 973) under grant No. 2007CB815401.

REFERENCES

Abel, T., Bryan, G. & Norman, M. L., 2000, ApJ, 540, 39.
 Abel, T., Bryan, G. L., & Norman, M. L. 2002, Science, 295, 93

³After the preprint of this paper was circulated, it was shown in Li, Zhang, & Chen (2007) that the angular size of the Ly α sphere can be magnified by gravitational lensing. For some strongly lensed system, the baseline could be reduced to about 10 km.

Allison, A. C. & Dalgarno, A., 1969, ApJ, 158, 423.
 Barkana, R., Loeb, A., 2001, Phys. Rep., 349, 125.
 Barkana, R., Loeb, A., 2005, ApJ, 626, 1.
 Barkana, R., Loeb, A., 2005, MNRAS, 363, L36.
 Bharadwaj, S., Ali, S. S., 2004, MNRAS, 142.
 Bromm, V., Coppi, P.S., Larson, R. B., 1999, ApJ, 527, 5.
 Bromm, V., Kudritzki, R. P., & Loeb, A., 2001, ApJ, 552, 464.
 Bromm, V., & Larson, R. B., 2004, ARA&A, 42, 79.
 Cen, R., 2003, ApJ, 591, 12.
 Cen, R., 2006, ApJ, 648, 47.
 Chen, X. & Miralda-Escudé, J., 2004, ApJ, 602, 1.
 Chen, X., & Kamionkowski, M., 2004, Phys. Rev. D, 70, 043502.
 Ciardi, B. & Ferrara, A., 2005, Space Sci. Rev., 116, 625.
 Ciardi, B. & Madau, P., 2003, ApJ, 596, 1.
 Cohn, J. D., & White, M., 2007, arXiv:0706.0208.
 Engeln-Mullges, G. & Uhlig, F., 1996, *Numerical Algorithms with C*, Springer, 1996.
 Field, G. B., 1959, ApJ, 129, 551.
 Furlanetto, S., 2006, MNRAS, 371, 867.
 Furlanetto, S. & Furlanetto, M., 2007a, MNRAS, 374, 547.
 Furlanetto, S. & Furlanetto, M., 2007b, MNRAS, 379, 130.
 Furlanetto, S., Oh, S. P., & Briggs, F. H., 2006, Phys. Rep., 433, 181.
 Furlanetto, S., Oh, S. P., & Pierpaoli, E., E., 2006, Phys. Rev. D74, 103502.
 Furlanetto, S. & Pritchard, J. R., 2006, MNRAS, 372, 1093.

- Furlanetto, S., Sokasian, A., Hernquist, L., 2004, MNRAS, 347, 187.
- Hirata, C., 2006, MNRAS, 367, 259.
- Hummer, D. G., Seaton, M. J., 1963, MNRAS, 125, 437.
- Hummer, D. G., Storey, P. J., 1998, MNRAS, 297, 1073.
- Iliev, I. T., Shapiro, P. R., Ferrara, A., Martel, H., 2002, ApJ, 572, L123.
- Iliev, I. T., Mellema, G., Pen, U.-L., Merz, H., Shapiro, P.R., Alvarez, M. A., 2006, MNRAS, 369, 1625.
- Jang-Condell, H., Hernquist, L., 2001, ApJ, 548, 68.
- Jenkins, A. et al., 2001, MNRAS, 321, 372.
- Kohler, K., Gnedin, N. Y., Miralda-Escudé, J., & Shaver, P. 2005, ApJ, 633, 552.
- Kuhlen, M., Madau, P., & Montgomery, R. 2006, ApJ, 637, 1
- Li, G., Zhang, P., Chen, X., 2007, ApJ, 666, 45.
- Loeb, A. & Rybicki, G. B., 1999, ApJ, 524, L527.
- Loeb, A. & Zaldarriaga, M., 2004, Phys. Rev. Lett., 92, 1301.
- Lukic, Z., Heitmann, K., Habib, S., Bashinsky S., Ricker, P. M., 2007, arXiv:astro-ph/0702360
- Madau, P., Meiksin, A., & Rees, M. J., 1997, ApJ, 475, 492.
- Miralda-Escudé, J., 2003, *Science*, 300, 1904.
- Mo, H.J. & White, S.D.M., 1996, MNRAS, 282, 347.
- Mo, H.J. & White, S.D.M., 2002, MNRAS, 336, 112.
- Naoz, S., Barkana, R., 2005, MNRAS, 362, 1047.
- Oh, S.P., ApJ, 553, 499.
- Omukai, K., & Palla, F. 2004, ApJ, 589, 677.
- Press, W., & Schechter, P., 1974, ApJ, 187, 425.
- Pritchard, J. R., & Furlanetto, S., 2006, MNRAS, 367, 1057.
- Pritchard, J. R., & Furlanetto, S., 2007, MNRAS, 376, 1680.
- Reed, D. et al, 2003, MNRAS, 346, 565.
- Reed, D. S. et al., 2005, MNRAS, 363, 393.
- Ripamonti, E., Mapelli, & M., Ferrara, A., 2007, MNRAS, 375, 1399.
- Santos, M.G., Cooray, A., & Knox, L., ApJ, 625, 575.
- Seager, S., Sasselov, D., & Scott, D. 2000, ApJS, 128, 407.
- Sethi, S. K., 2005, MNRAS, 363, 818.
- Sheth, R. K. & Tormen, G., 1999, MNRAS, 308, 119.
- Shull, M. & van Steenberg, 1985, ApJ, 298, 268.
- Storey, P. J., & Hummer, D. G., 1995, MNRAS, 272, 41.
- Thompson, A.R., Moran, J.M., Swenson, G.W. Jr., 2001, *Interferometry and synthesis in radio astronomy*, 2nd.ed., Wiley, New York.
- Tozzi, P., Madau, P. Meiksin, A., & Rees, M. J., 2000, ApJ, 528, 597.
- Valdes, M., Ferrara, A., Mapelli, M., Ripamonti, E., 2007, MNRAS, 377, 245.
- Verner, D.A., Ferland, G.J., Korista, K.T., Yakovlev, D.G., 1996, ApJ, 465, 487.
- Warren, M. S., Abazajian, K., Holz, D., Teodoro, L., 2006, ApJ, 646, 881.
- Whalen, D., Abel, T., Norman, M. L., 2004, ApJ, 610, 14.
- Woosley, S. E., Heger, A., Weaver, T. A., 2002, RMP, 74, 1015.
- Wouthuysen, S. A., 1952, AJ, 57, 31.
- Yoshida, N., Abel, T., Hernquist, L., Sugiyama, N., 2003, ApJ, 592, 645.

Zahn, O., Lidz, A., McQuinn, M., Dutta, S., Hernquist, L., Zaldarriaga, M., Furlanetto, S. R., ApJ, 654, 12.

Zygelman, B., 2005, ApJ, 622, 1356.

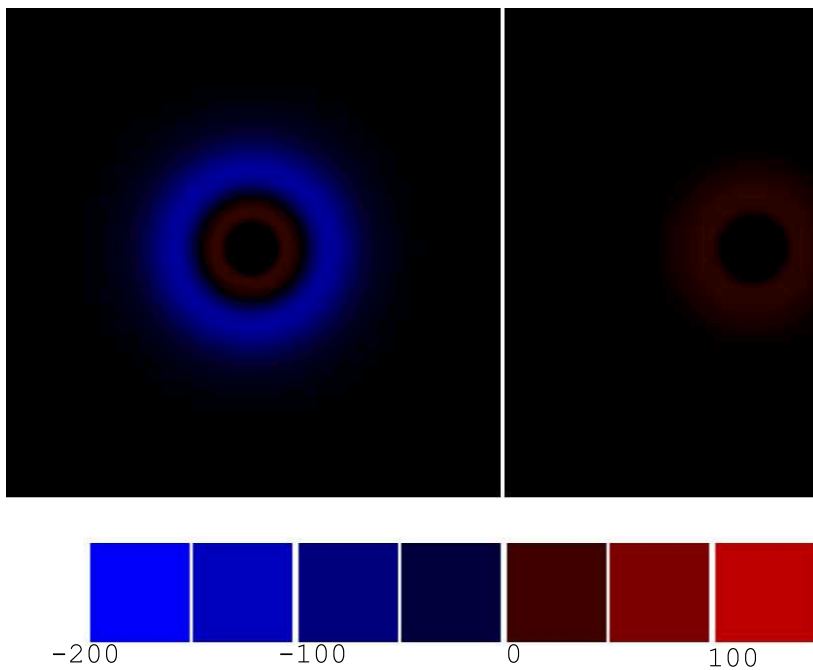


Fig. 17.— A cross section map for a star of $200 M_{\odot}$ and age 1.5 Myr at redshift 20(left) and 15(right). The box size is 40 kpc across (physical distance), and unit of temperature scale is mk.